Rare Metal Materials and Engineering
Volume 55, Issue 1, January 2026
Available online at www.rmme.ac.cn

Science Press

Cite this article as: Yang Fan, Chang Jianxiu, Wang Xin, et al. Effect of Substrate Micro-arc Oxidation Pretreatment on Microstructure and High-Temperature Oxidation Resistance of Si-Cr-Ti-Zr Coating on Ta12W Alloy[J]. Rare Metal Materials and Engineering, 2026, 55(01): 92-104. DOI: https://doi.org/10.12442/j.issn.1002-185X.20250319.

ARTICLE

Effect of Substrate Micro-arc Oxidation Pretreatment on Microstructure and High-Temperature Oxidation Resistance of Si-Cr-Ti-Zr Coating on Ta12W Alloy

Yang Fan[1,2], Chang Jianxiu[1], Wang Xin[2], Li Hongzhan[2], Yan Peng[2]

[1] School of Materials Science and Engineering, Xi'an Shiyou University, Xi'an 710065, China; [2] Northwest Institute for Nonferrous Metal Research, Xi'an 710016, China

Abstract: To mitigate the impact of interdiffusion reactions between the silicide slurry and Ta12W alloy substrate during vacuum sintering process on the oxidation resistance of the silicide coating, a micro-arc oxidation pretreatment was employed to construct a Ta_2O_5 ceramic layer on the Ta12W alloy surface. Subsequently, a slurry spraying-vacuum sintering method was used to prepare a Si-Cr-Ti-Zr coating on the pretreated substrate. Comparative studies were conducted on the microstructure, phase composition, and isothermal oxidation resistance (at 1600 ℃) of the as-prepared coatings with and without the micro-arc oxidation ceramic layer. The results show that the Ta_2O_5 layer prepared at 400 V is more continuous and has smaller pores than that prepared at 350 V. After micro-arc oxidation pretreatment, the Si-Cr-Ti-Zr coating on Ta12W alloy consists of three distinct layers: an upper layer dominated by Ti_5Si_3, Ta_5Si_3, and ZrSi; a middle layer dominated by $TaSi_2$; a coating/substrate interfacial reaction layer dominated by Ta_5Si_3. Both the Si-Cr-Ti-Zr coatings with and without the Ta_2O_5 ceramic layer do not fail after isothermal oxidation at 1600 ℃ for 5 h. Notably, the addition of the Ta_2O_5 ceramic layer reduces the high-temperature oxidation rate of the coating.

Key words: tantalum-tungsten alloy; silicide coating; micro-arc oxidation; reaction formation mechanism; high-temperature oxidation

1 Introduction

With the continuous advancement of the aerospace industry and nuclear engineering technologies, high-temperature structural materials represented by nickel-based superalloys can no longer meet the ever-increasing temperature requirements of advanced applications. For instance, the hot-end temperature of a new generation of high-performance orbit-control rocket engines exceeds 1650 ℃[1], which is much higher than the service temperature range of nickel-based single crystal superalloys (850 – 1150 ℃) [2–3]. Refractory metals, such as niobium (Nb), tungsten (W), molybdenum (Mo), tantalum (Ta), and rhenium (Re), have melting points above 2000 ℃ and are widely used in electronics, chemical industry, military, aerospace, and other fields[4]. Among these, pure Ta exhibits an outstanding balance of high melting point (2996 ℃), high-temperature tensile strength, and low-temperature plasticity[5–6]. Adding another refractory element (W) into Ta enables property enhancement of pure Ta through solid-solution strengthening: the newly formed Ta-W alloy not only retains the excellent plasticity and corrosion resistance of pure Ta, but also exhibits enhanced hardness and ablation resistance. Furthermore, as the W content increases, the room-temperature tensile strength and strain hardening rate of the Ta-W alloy also further increase[7]. Ta-W alloy has been extensively applied in the aerospace field, particularly in hypersonic vehicles, engine combustion chambers, and rocket thrust chambers[8–9]. However, when the service temperature exceeds 500 ℃, severe oxidation occurs on the alloy surface, resulting in the formation of porous Ta_2O_5. Due to the large Pilling-Bedworth ratio (PBR) of Ta_2O_5 (PBR_{Ta}=2.484), the growth stress of the oxide layer is large. During the thickening

Received date: June 09, 2025
Foundation item: National Natural Science Foundation of China (52071274); Key Research and Development Projects of Shaanxi Province (2023-YBGY-442); Science and Technology Nova Project-Innovative Talent Promotion Program of Shaanxi Province (2020KJXX-062)
Corresponding author: Wang Xin, Ph. D., Professor, Northwest Institute for Nonferrous Metal Research, Xi'an 710016, P. R. China, E-mail: wangx@alum.imr.ac.cn; Chang Jianxiu, Ph. D., Professor, School of Materials Science and Engineering, Xi'an Shiyou University, Xi'an 710065, P. R. China, E-mail: jxchang11s@alum.imr.ac.cn

process, the oxide film may crack and spall off, leading to catastrophic oxidation[10–11]. The insufficient high-temperature oxidation resistance severely restricts the application of Ta-W alloy in aviation, aerospace, and nuclear industries. Therefore, improving the high-temperature oxidation resistance of Ta-W alloy is crucial[12].

At present, the most commonly used methods for high-temperature protection involve the addition of antioxidant elements and the application of high-temperature oxidation-resistant coatings[13]. However, alloying elements have a limited effect on improving oxidation resistance, and excessive addition may even degrade the mechanical properties of the matrix[14]. Applying high-temperature oxidation-resistant coatings can effectively enhance the oxidation resistance of the matrix without degrading its mechanical properties. Currently, high-temperature oxidation-resistant coatings can be broadly categorized into five categories: precious metal coatings, alloy coatings, oxide ceramic coatings, aluminide coatings, and silicide coatings[15]. The protection mechanism of precious metal coatings is purely physical barriers (no chemical reactions), which can enhance the corrosion resistance, oxidation resistance, and ductility of the matrix. They also exhibit extremely low oxygen permeability and oxide evaporation rates. However, their high cost significantly restricts widespread application[16]. Alloy coatings primarily rely on the formation of a dense oxide film through the reaction between alloying elements and oxygen during oxidation, thereby hindering the diffusion of metal cations and oxygen. Alloy coatings have advantages such as small thickness, good plasticity, and excellent adhesion in service. However, their service temperature is limited to below 1200 ℃[17]. Besides, they exhibit poor high-temperature self-healing capabilities. Oxide ceramic coatings possess numerous excellent characteristics, such as high melting points, good chemical stability, and ablation resistance. These coatings effectively protect the matrix relying on the low diffusion rate and long diffusion path of oxygen within the coating, as well as their non-reactivity with the matrix. However, the large thickness and brittleness of oxide ceramic coatings increase the spallation tendency during service, ultimately leading to coating failure. The oxidation resistance mechanism of aluminide coatings is based on the reaction of highly reactive Al with oxygen, which can form a dense Al_2O_3 film. Al_2O_3 exhibits high stability and density at high temperatures, effectively blocking oxygen permeation. Additionally, due to the low growth rate of the Al_2O_3 film, aluminide coatings can have a longer service life[18–20].

In the field of high-temperature protection for refractory metals, silicide coating systems have become the most widely used coatings due to their unique advantages. Their oxidation resistance stems from the reaction between silicides and oxygen, resulting in the formation of a complete and dense SiO_2 film[21]. Furthermore, the fluidity of SiO_2 at high temperatures resolves the defects, such as holes and cracks in the coating, endowing the coating with "self-healing" properties that effectively block oxygen penetration. Additionally, the diffusion rate of oxygen in SiO_2 is very low, which contributes to the excellent high-temperature oxidation resistance of the coating[22]. Furthermore, silicide coating system has a high-temperature tolerance limit (about 1800 ℃). This characteristic renders it particularly well-suited for the ultra-high-temperature service environments of refractory metals[23]. The Si-Cr-Ti coating system was firstly developed by NASA. In 1994, researchers from Beihang University and Tsinghua University modified the Si-Cr-Ti coating on C-103 Nb-based alloy by adding Zr. Their findings showed that Zr addition significantly enhanced the oxidation resistance of the coating[24]. Most importantly, a mature coating preparation technology system has been developed for silicide coatings. Among these, the slurry spraying-vacuum reaction sintering method has distinct advantages: easy control of coating composition, a simple preparation process, and the ability to achieve uniform coatings on complex irregular workpiece surfaces. It is currently the most widely used process for preparing coatings on refractory metal surfaces[25].

However, during the preparation of coatings using the slurry spraying-vacuum reaction sintering method, Si in the coating inevitably undergoes a high-temperature diffusion reaction with the matrix, resulting in the predominance of Ta-Si phases in the coating[26]. Due to the high affinity of Ta, Si, and oxygen for one another, the Ta-Si ceramics in the outer layer of the coating, especially the medium-silicon phase, undergo oxidation, leading to the formation of glassy SiO_2 mixed with a large amount of Ta_2O_5 in the coating. This impairs the oxygen resistance of the oxide film, thereby diminishing the overall oxidation resistance of the coating.

This study aimed to slow the diffusion of Si from the slurry pre-layer to the matrix side during vacuum reaction sintering and inhibit reactions between matrix elements and Si. Firstly, a porous Ta_2O_5 oxide ceramic layer was prepared on a Ta12W substrate using micro-arc oxidation (MAO). Then, a Si-Cr-Ti-Zr coating was prepared on the surface of the Ta12W alloy using the slurry spraying-vacuum reaction sintering method. This design prioritized reactions between metal elements in the slurry pre-coating and Si to form corresponding silicide ceramic phases, thereby regulating the structure and phase composition of the outer layer of the coating, as well as the structure and phase of the oxide film, and thus enhancing the oxidation resistance of the coating under high-temperature conditions. To clarify how MAO ceramic layer affects coating structure, microstructure, and high-temperature oxidation resistance, a control group was set up: a Si-Cr-Ti-Zr coating was prepared directly on the Ta12W alloy surface (without the MAO layer) using the same slurry spraying-vacuum reaction sintering method, and its isothermal oxidation resistance was tested under identical conditions. By comparing the microstructure, phase composition, and isothermal oxidation resistance (at 1600 °C) of the coatings with and without the Ta_2O_5 oxide ceramic layer, the influence of the Ta_2O_5 layer on the coating's reaction formation mechanism and high-temperature oxidation resistance was discussed.

2 Experiment

2.1 Material preparation

In this study, a tantalum-based alloy (Ta12W) supplied by Xi'an Noble Precious Metal Materials Co., Ltd was selected as the matrix material. Firstly, the Ta12W alloy was cut into strip-shaped specimens with dimensions of 70 mm×10 mm×1.5 mm using a wire cutter. Subsequently, the specimens were polished and chamfered with 320# and 600# sandpapers. To increase the surface roughness and improve coating adhesion, the specimens were then sandblasted using a sandblasting machine (model 9060E, Suzhou Baide Sandblasting Machinery Company). After sandblasting, the sandblasted substrates were immersed in an ethyl acetate solution and ultrasonically cleaned for 20 min to remove residual corundum sand from their surfaces. Finally, the specimens were acid-pickled for subsequent experiments.

For slurry preparation, Si, Cr, Ti, and Zr powders (particle size: 1–5 μm; purity: ≥99.9%) were purchased from Shanghai Naio Nano Technology Co., Ltd. Sodium hydroxide (NaOH) used in the MAO experiment was sourced from Sinopharm Chemical Reagent Shaanxi Co., Ltd.

2.2 Coating preparation

2.2.1 Ta_2O_5 oxide ceramic layer preparation

A Ta_2O_5 oxide ceramic layer was prepared via the MAO method. Firstly, an electrolyte was prepared using a NaOH solution with a concentration of 10 g/L. Then, the pretreated Ta12W specimens were placed in an electrolytic cell, and MAO was performed using a T-25Z thick-film oxidizer (developed by the Northwest Institute for Nonferrous Metals Research). The cathode was a stainless-steel plate. The process parameters were as follows: pulse voltage of 350–400 V, duty cycle of 20%, temperature controlled below 45 °C, discharge frequency of 1000 Hz, and oxidation duration of 20 min. By adjusting the discharge voltage, the Ta_2O_5 oxide ceramic layer was prepared[27–29].

2.2.2 Silicide coating preparation

The silicide coating was prepared using the slurry spraying-vacuum reaction sintering method. Firstly, Si-Cr-Ti-Zr powders were weighed proportionally as the coating material using an electronic balance, and an appropriate amount of dispersant was added. Then, the mixture was placed in an agate-filled ball milling jar for high-energy ball milling to prepare the silicide coating slurry. The ball milling speed was 340 r/min, with a duration of 48 h. Subsequently, the slurry was uniformly sprayed onto the surface of the Ta12W alloy using a pneumatic spraying method. Then, the specimens with the pre-coated slurry layer were dried at 80 °C for 15 min. Finally, the dried specimens were placed in a vacuum sintering furnace, heated to 1420 °C at a rate of 10 °C/min, held at this temperature for 1 h, and then naturally cooled in the furnace. The specific flow chart is shown in Fig.1.

2.3 Oxidation test

A self-made device was used to conduct an isothermal oxidation test on the coating at 1600 ℃. As shown in Fig.2, in the atmospheric environment, by applying a high current, the specimens were heated from room temperature to 1600 ℃ at a rate of 600 ℃/min. To evaluate the ultra-high-temperature oxidation resistance of the coating, the system automatically recorded the duration from the start of the isothermal holding period to the coating failure period. In addition, to preserve the oxidized coatings and prevent cracking during specimen preparation, the surface of the oxidized specimen was plated with nickel.

2.4 Characterization

The phase composition of the coatings was determined by X-ray diffractometer (XRD; Panalytical X' Pert PRO, PANalytical, Almelo, Netherlands) with Cu Kα radiation (operating at 40 kV). XRD analyses were performed over a 2θ range from 20° to 80° at a scanning rate of 2°/min. Qualitative and quantitative analyses of the coating surface and cross-section before and after oxidation were performed using a field emission scanning electron microscope (SEM; SU-5000, Oxford Instruments, Oxford, U.K.) equipped with an energy dispersive X-ray spectrometer (EDS; X-Max, Oxford Instruments Co., Oxford, U.K.). The thermodynamic reaction equation was investigated using a commercial software package (HSC Chemistry v.6.0).

3 Results

3.1 Phase and microstructure of as-prepared Si-Cr-Ti-Zr coating on Ta12W alloy

Fig.3 presents XRD patterns of the as-prepared Si-Cr-Ti-Zr

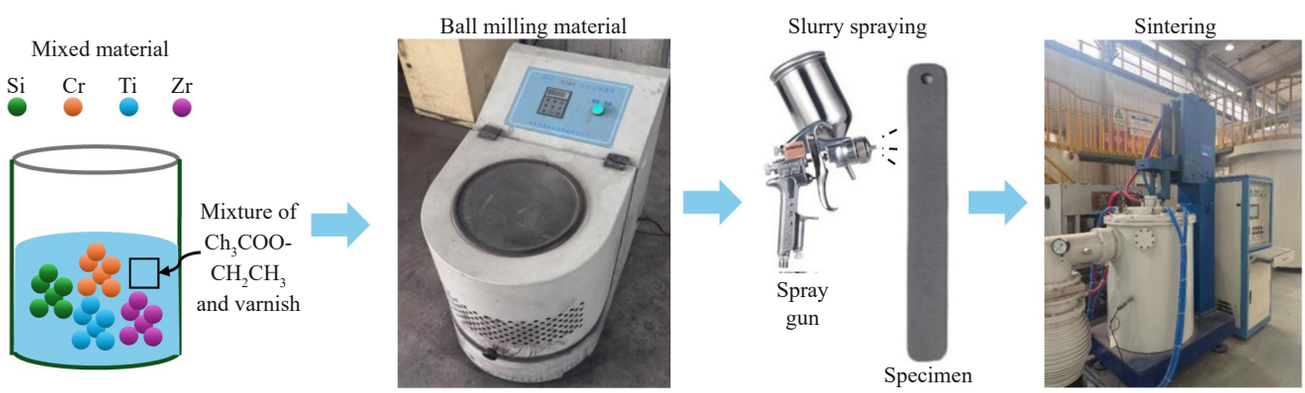

Fig.1 Schematic diagram of the slurry spraying-vacuum sintering coating preparation process

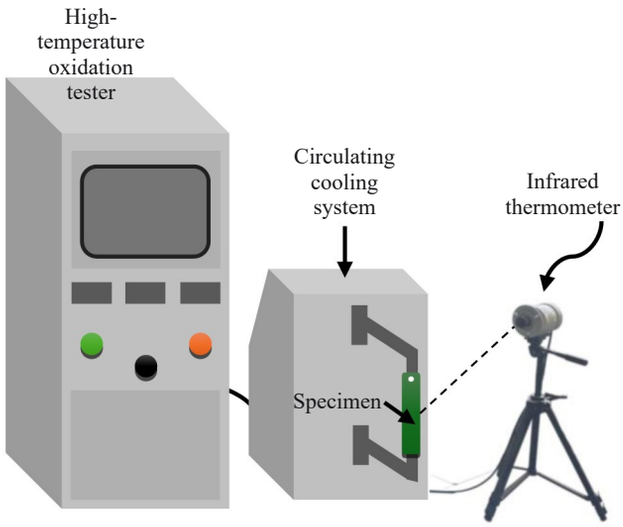

Fig.2 Schematic diagram of isothermal oxidation test

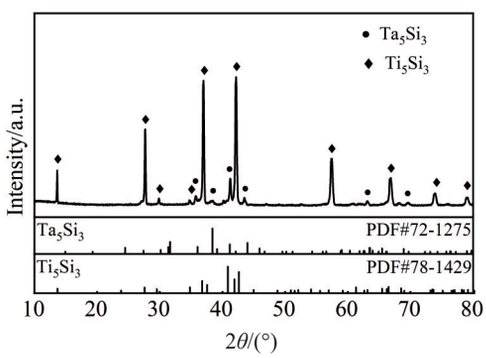

Fig. 3 XRD patterns of Si-Cr-Ti-Zr coating on Ta12W alloy surface and related composition phases

coating. The surface phases of the coating are primarily Ti_5Si_3 and Ta_5Si_3. Fig. 4 illustrates the surface and cross-section morphologies of the as-prepared coating, along with the corresponding EDS results. As shown in Fig. 4a, the coating surface exhibits high compactness with no evident defects. The as-prepared coating surface consists of three main morphologies: rod-like, granular, and planar regions. It is worth noting that $TaSi_2$ diffraction peaks are not detected in XRD analysis. This is likely because the coating surface is mainly composed of rod-shaped Ta_5Si_3, while the content of granular $TaSi_2$ is relatively low, with most of it located below the rod-shaped particles. Due to its weak diffraction intensity, the $TaSi_2$ phase is not detected. However, EDS point analysis of the particle phase in the coating yields the data for point 3, as shown in Table 1. In summary, it can be reasonably inferred that the main phase of the rod-shaped and planar structures on the coating surface is Ti_5Si_3, while the main phase of the granular structure is (Ta, Ti)Si_2. The cross-section morphology of the coating (Fig. 4b) reveals a three-layer structure, with significant differences in morphology among the outer, middle, and bottom layers. The outer layer exhibits typical equiaxed crystal characteristics, has a thickness of approximately 38 μm, and it is predominantly enriched in Cr, Ti, and Zr. The middle silicide layer, with a thickness of approximately 42 μm, consists mainly of the $TaSi_2$ phase, with a small amount of white Ta_5Si_3 particles mixed in its inner region. Additionally, an interfacial reaction layer of approximately 3.7 μm exists at the coating/substrate interface, and its phase is identified as Ta_5Si_3. The high-magnification image of the middle layer in Fig. 4b is illustrated in Fig. 4c. Combined with EDS results of Fig. 4c, the dark gray region is predominantly enriched in Cr. Based on EDS results, the main phase in the dark gray region is inferred to be Cr_5Si_3. The light gray region is identified as $TaSi_2$ based on the results of point 4 and the Ta-Si phase diagram. The gray region, which is enriched in Zr, is identified as ZrSi based on the point data and the Zr-Si phase diagram.

3.2 Phase and microstructure of as-prepared Si-Cr-Ti-Zr coating on Ta12W alloy after MAO pretreatment

3.2.1 Phase composition and morphology of MAO ceramic layer

Fig. 5 displays XRD patterns of Ta_2O_5 oxide ceramic layers prepared by MAO on the surface of Ta12W alloy under different discharge voltages. The coating mainly consists of Ta_2O_5 and Ta. Fig. 6a and 6b present the surface morphologies of Ta_2O_5 oxide ceramic layers prepared by MAO at 350 and 400 V, respectively. Both surfaces are completely covered by a continuous porous Ta_2O_5 oxide ceramic layer. However, the pore diameters in Fig. 6b are smaller than those in Fig. 6a. Fig. 6c and 6d show the cross-section morphologies of the Ta_2O_5 oxide ceramic layers at voltages of 350 and 400 V, respectively. Both Ta_2O_5 layers have a thickness of approximately 7 μm. The pores in Fig. 6d are smaller than those in Fig. 6c, and the Ta_2O_5 oxide ceramic layer in Fig. 6d is more continuous and denser, which is consistent with the surface observations.

3.2.2 Phase analysis of as-prepared Si-Cr-Ti-Zr coating on Ta12W alloy after MAO treatment

Fig. 7 displays XRD patterns of Si-Cr-Ti-Zr coatings prepared on the surface of Ta12W alloy after MAO pretreatment at different voltages. The coating surface mainly consists of Ti_5Si_3, ZrSi, and Ta_5Si_3.

The surface and cross-section morphologies of the Si-Cr-Ti-Zr coatings prepared on the surface of Ta12W alloy after MAO pretreatment at 350 V are illustrated in Fig. 8, along with EDS results. As shown in Fig. 8a, the coating is primarily composed of rod-like structures and aggregated granular particles. The grains of the rod-like structures are relatively fine. Cracks can also be observed on the coating surface. As depicted in Fig. 8b, the cross-section morphology of the as-prepared coating can be divided into three layers: the outer layer of the coating (thickness of approximately 22 μm), the inner layer of the coating (thickness of approximately 35 μm), and the coating/substrate interfacial reaction layer (thickness of approximately 6 μm). The coating exhibits various morphological characteristics, and the outer layer has a relatively undulating morphology. Combining XRD and SEM results,

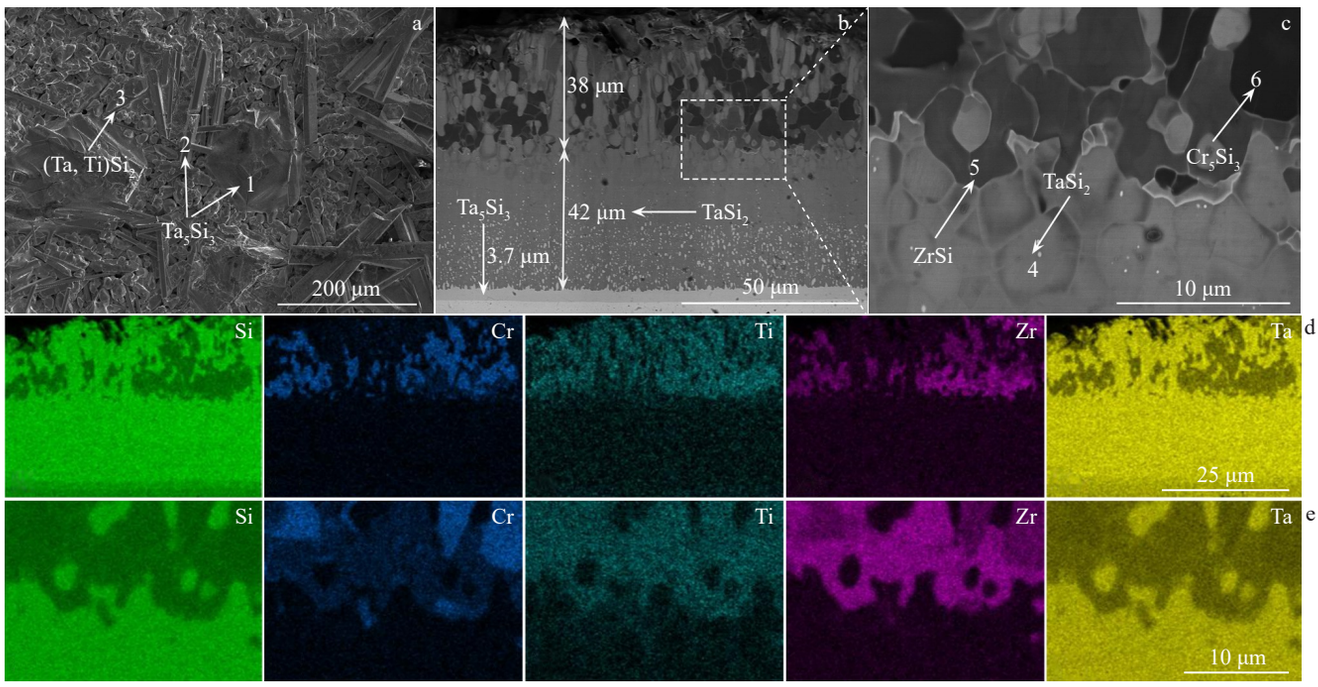

Fig.4 Surface (a) and cross-section (b–c) morphologies of Si-Cr-Ti-Zr coatings; EDS elemental mappings corresponding to Fig.4b (d) and Fig.4c (e)

Table 1 EDS results of points marked in Fig.4

Point	Element content/at%						Main phase
	Si	Cr	Ti	Zr	Ta	W	
1	43.83	8.23	29.09	9.33	8.41	1.10	Ti_5Si_3
2	39.85	11.79	28.02	8.76	10.73	0.85	Ti_5Si_3
3	67.38	3.34	11.74	1.11	14.77	1.66	$(Ta, Ti)Si_2$
4	67.99	0.89	0.90	3.65	26.07	0.50	$TaSi_2$
5	46.33	11.40	11.06	19.94	10.40	0.88	ZrSi
6	45.65	29.86	8.40	10.29	5.16	0.63	Cr_5Si_3

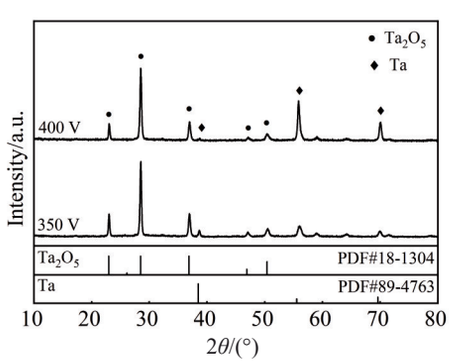

Fig.5 XRD patterns of Ta_2O_5 layers on Ta12W alloy surface with MAO pretreatment at different voltages

the outer layer is composed of Ti_5Si_3, Ta_5Si_3, Cr_5Si_3, and ZrSi; the inner layer is $TaSi_2$; the reaction layer is Ti_5Si_3. Furthermore, the SEM-EDS surface analysis results indicate that Ti is predominantly enriched in the outer layer, accompanied by trace enrichments of Cr and Zr. Notably, no Ta_2O_5 oxide ceramic layer is observed at the coating/substrate interface.

Fig.9 illustrates the surface and cross-section morphologies of the Si-Cr-Ti-Zr coating prepared on the Ta12W alloy surface after MAO pretreatment at 400 V, along with EDS results. EDS results of points marked in Fig. 9 are listed in Table 2. As revealed in Fig.9a, the coating surface consists of three main morphologies: rod-like structures, fine particles, and planar regions. XRD and EDS point analyses indicate that the main phases are as follows: $(Ti, Ta)_5Si_3$ in the rod-like structures, ZrSi in the planar regions, and $TaSi_2$ in the granular structures. Referring to Fig. 9b and its EDS area scan results, the cross-section of the coating primarily consists of three parts, with a total thickness of approximately 121 μm: outer layer (approximately 83 μm), inner layer (approximately 34 μm), and the coating/substrate interfacial reaction layer (approximately 4 μm). Notably, Ti_5Si_3 and Ta_5Si_3, as key oxidation-resistant phases, can form dense SiO_2 and TiO_2 protective films in high-temperature oxidation environments, effectively blocking oxygen diffusion to the matrix. Meanwhile, the Cr_5Si_3 phase and ZrSi phase enhance the stability of the oxide film by generating Cr_2O_3 and ZrO_2. Compared to the coating prepared with MAO pretreatment at 350 V (Fig.8b), the 400 V-treated coating exhibits two distinct advantages: (1) significantly improved sintering uniformity of the outer layer, which is the main component of the coating; (2) a marked reduction in thickness of the reaction layer, from 9.5% to 3.3%. Based on these advantages, the coating prepared with MAO pretreatment at 400 V was selected for subsequent oxidation experiments.

3.3 High-temperature isothermal oxidation behavior of Si-Cr-Ti-Zr coatings

Fig. 10 shows the macroscopic morphologies of the Si-Cr-Ti-Zr coating before and after isothermal oxidation at 1600 ℃

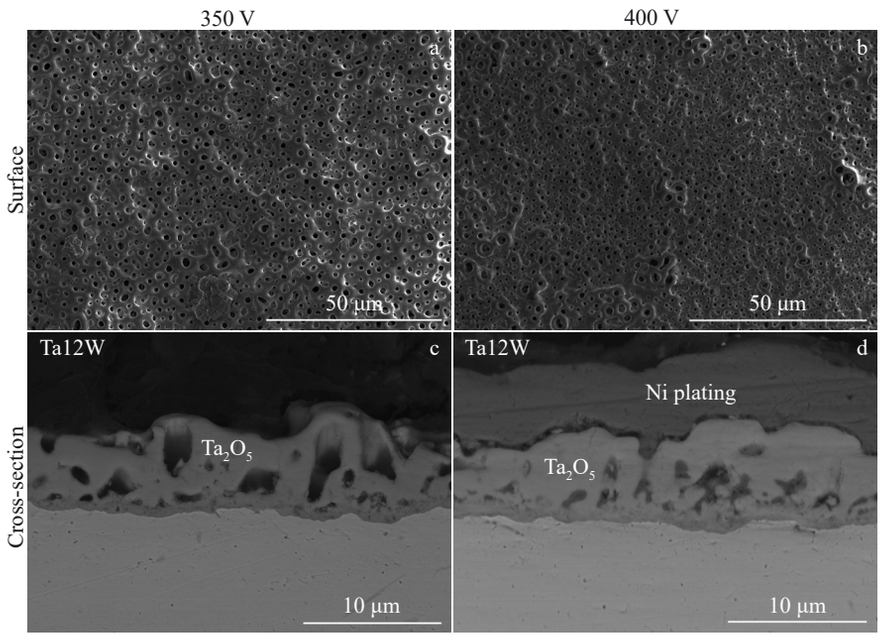

Fig.6 Surface (a–b) and cross-section (c–d) morphologies of Ta_2O_5 layers on Ta12W alloy surface with MAO pretreatment at different voltages

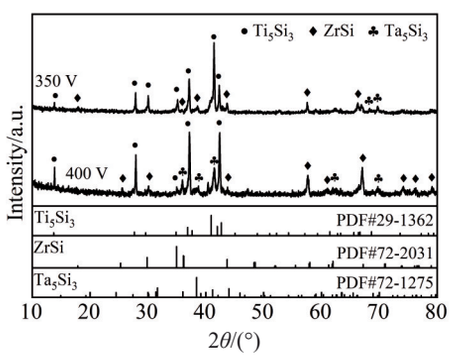

Fig.7 XRD patterns of Si-Cr-Ti-Zr coatings on Ta12W alloy surface with MAO pretreatment at different voltages

for 5 h. Before oxidation, the coating surface exhibits a noticeable glossy appearance. After oxidation, the color of the high-temperature area in the center of the specimen darkens significantly, and local spallation occurs in the transition zone between the high- and low-temperature areas, accompanied by the formation of a small amount of white oxide product.

Fig. 11 shows XRD pattern of Si-Cr-Ti-Zr coating oxidized at 1600 ℃ for 5 h. It can be seen that the oxides on the surface of the coating are mainly TiO_2 and SiO_2.

Fig. 12 shows the surface and cross-section morphologies of the coating after 5 h of oxidation, as well as corresponding EDS analysis results. As shown in Fig. 12a, the rod-shaped and granular phases on the coating disappear after 5 h of oxidation. Instead, small gray particles are dispersed on the dark black glassy film on the coating surface. EDS point analysis and XRD patterns jointly confirm that the glassy film is mainly composed of amorphous SiO_2, accompanied by a small number of crystalline SiO_2 particles, while the attached small particles are crystalline TiO_2. Fig. 12b clearly shows that the cross-section morphology of the coating after oxidation can be divided into four layers: an oxide layer (thickness of about 45 μm), the remaining coating (thickness of about 81 μm), a coating/substrate interfacial reaction layer (thickness of about 18 μm), and the substrate. The gray phase in the outer oxide layer is TiO_2, and the black phase is SiO_2, consistent with XRD results. Based on Fig. 12c and its EDS area scan results, it can be seen that the oxide Cr_2O_3 is distributed above the $TaSi_2$ phase. The main phase of the coating changes from $(Ti, Ta)_5Si_3$ (before oxidation) to $TaSi_2$ phase (after oxidation). Zr enrichment appears inside $TaSi_2$. The thickness of the interfacial reaction layer between the coating and the substrate also increases from 3 μm (before oxidation) to 18 μm (after oxidation). Additionally, according to cross-section images of the oxidized coating, the distribution of silicon phases in Ta_5Si_3 indicates that the coating degradation preferentially begins at the grain boundaries of $TaSi_2$ grains.

3.4 High-temperature isothermal oxidation behavior of Si-Cr-Ti-Zr coating on Ta12W alloy with MAO pretreatment at 400 V

Fig. 13 shows the macroscopic morphologies of Si-Cr-Ti-Zr coatings on Ta12W alloy surface pretreated by MAO at 400 V before and after oxidation at 1600 ℃ for 5 h. Before oxidation, the specimen surface is gray, with white particles evenly distributed. After oxidation, the central high-temperature zone of the specimen changes to dark brown, and a small amount of white oxide product appears. Compared to the coatings without MAO pretreatment (Fig. 10), the MAO-pretreated coatings have a lower degree of oxidation. Fig. 14 shows XRD pattern of the Si-Cr-Ti-Zr coating prepared on the Ta12W alloy surface with MAO pretreatment at 400 V after oxidization at 1600 ℃ for 5 h. Compared with XRD patterns of the Si-Cr-Ti-Zr coatings without MAO pretreatment,

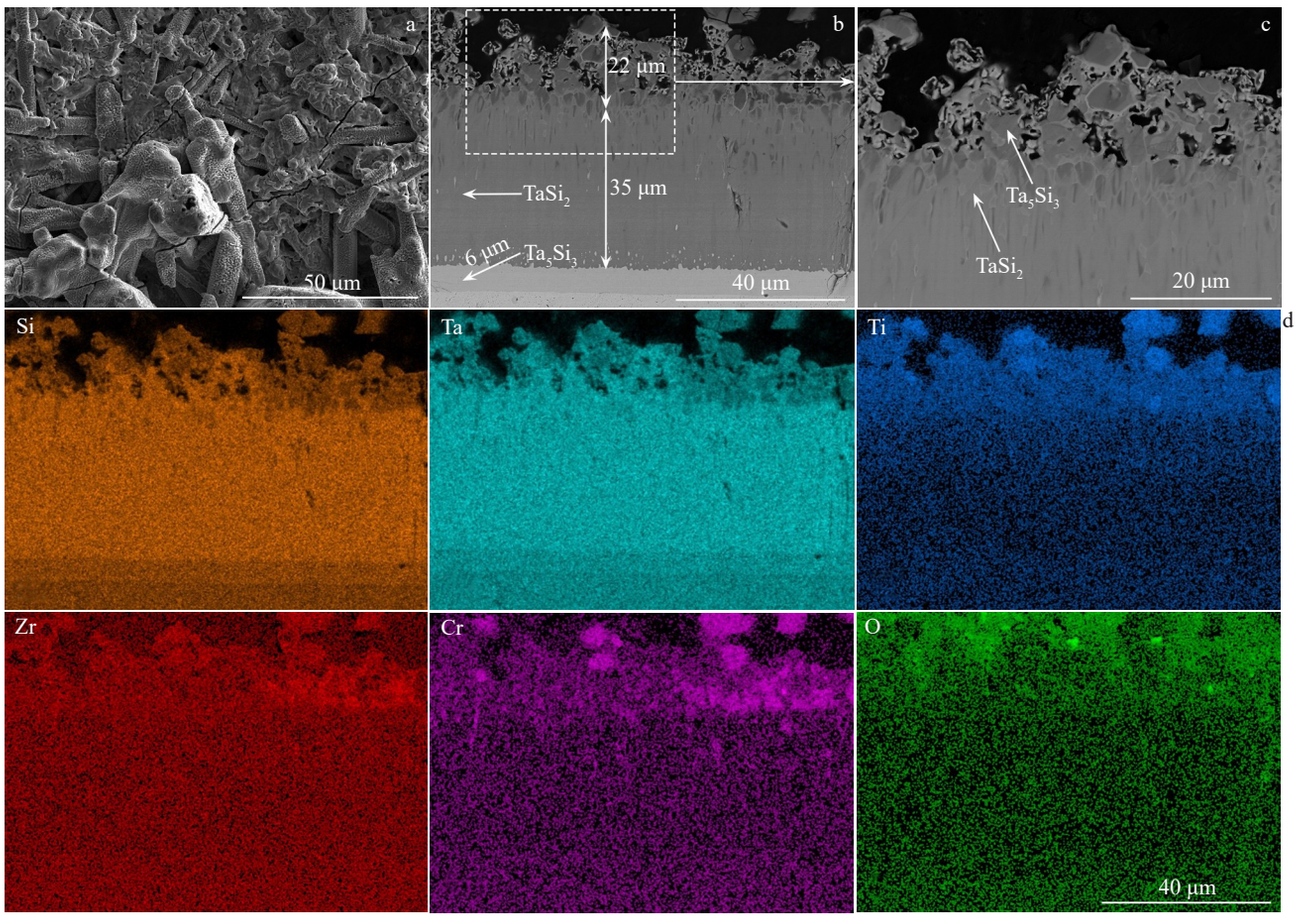

Fig.8 Surface (a) and cross-section (b–c) morphologies of Si-Cr-Ti-Zr coating on Ta12W alloy surface with MAO pretreatment at 350 V; EDS element mappings corresponding to Fig.8b (d)

diffraction peaks of $TiTaO_4$ are detected in this MAO-pretreated coating (with the additional Ta_2O_5 oxide ceramic layers), but diffraction peaks of crystalline TiO_2 are absent. Fig. 15 shows the surface and cross-section morphologies as well as EDS area scan results of MAO-pretreated (400 V) Si-Cr-Ti-Zr coating. As shown in Fig. 15a, the surface morphology of the coating does not undergo significant changes after oxidation at 1600 ℃ for 5 h, and the rod-shaped structure on the coating surface does not completely disappear after oxidation. Compared to the surface of the coating before oxidation, there is a significant reduction in microcracks on the surface after oxidation. This is due to the high-temperature fluidity of SiO_2, which can fill the cracks and gaps in the coating. Compared with Fig. 12a (surface morphology of the silicide coating without Ta_2O_5 oxide ceramic layer after 5 h of oxidation), the surface oxidation degree of the MAO-pretreated coating (with Ta_2O_5 layer) is lower.

Fig. 15b shows the cross-section morphology of the coating after oxidation, which can be divided into three layers: an oxide layer (thickness of about 125 μm), a remaining coating layer (thickness of about 109 μm), and a coating/substrate interfacial reaction layer (thickness of about 31 μm). Notably, there are still a few coating materials remaining in the oxide layer. Combined with XRD results, the gray phase in the oxide layer is identified as $TiTaO_4$, and the black phase is SiO_2. Based on Fig. 15c, it can be concluded that the light gray phase above the coating is mainly Ta_5Si_3, and the dark gray phase is mainly $TaSi_2$. Cr_2O_3 is distributed at the interface between the coating and the oxide layer, while ZrO_2 is still embedded in the topmost layer of the coating. However, unlike the coating without Ta_2O_5 oxide ceramic layer after oxidation, $ZrSiO_4$ is found in the oxide layer after adding Ta_2O_5 oxide ceramic layer.

4 Discussion

4.1 In-situ reaction formation mechanism of Si-Cr-Ti-Zr coating

In this study, the Si-Cr-Ti-Zr coating was sintered in a vacuum environment at 1420 ℃. Once sintering was initiated, Si powder in the pre-coated layer melted and wetted both the metal powders (Cr, Ti, and Zr) in the pre-layer and the Ta12W alloy matrix, triggering a series of high-temperature interfacial diffusion reactions and thus forming corresponding silicide phases. However, the coating had different element-enriched regions, which can be attributed to three key factors: significant differences in the diffusion coefficients of different elements in the silicide ceramic layer, varying affinity between different metal elements and Si, and differences in

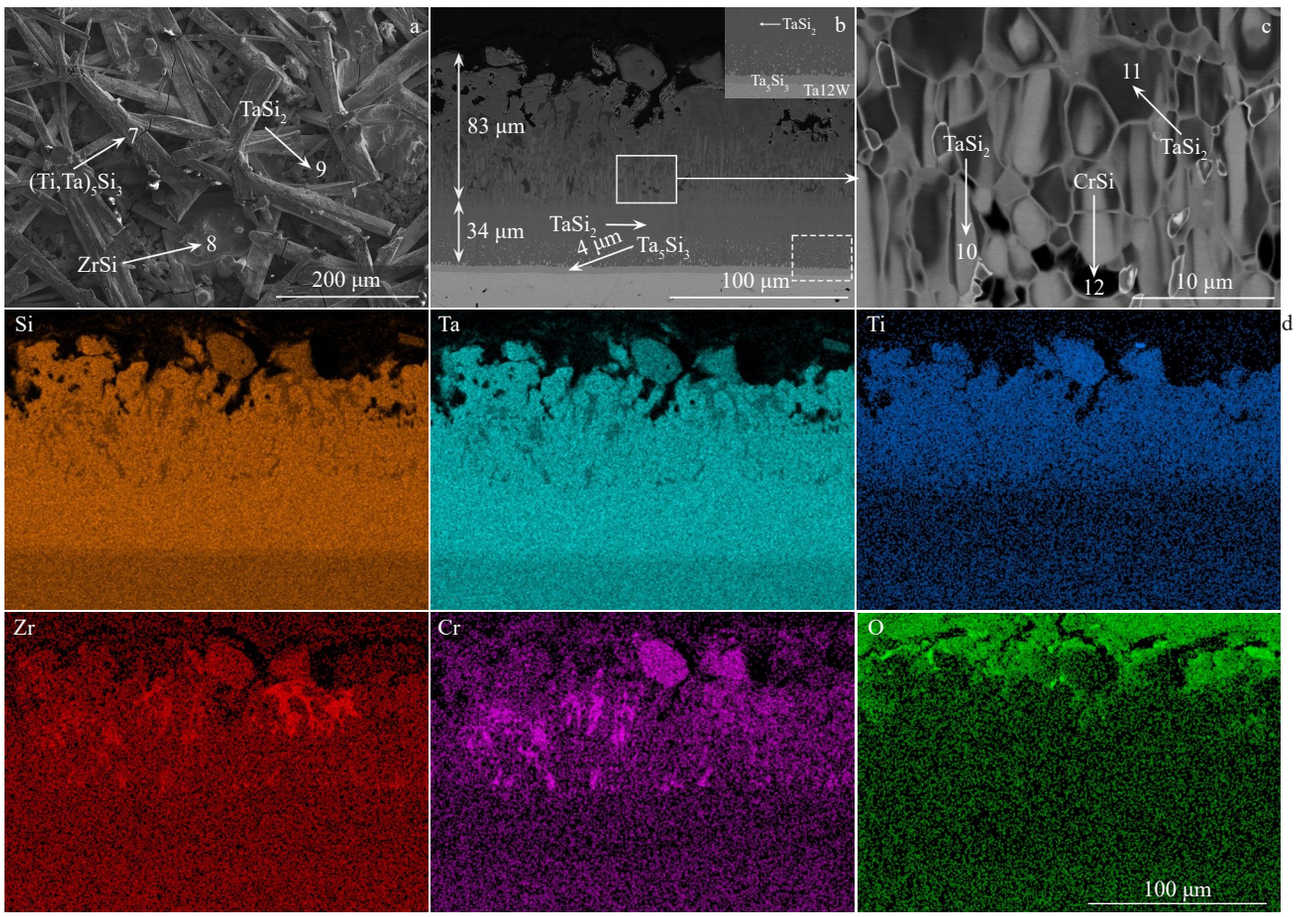

Fig.9 Surface (a) and cross-section (b–c) morphologies of Si-Cr-Ti-Zr coating on Ta12W alloy with MAO pretreatment at 400 V; EDS element mappings corresponding to Fig.9b (d)

Table 2 EDS scanning results of points marked in Fig.9

Point	Element content/at%						Main phase
	Si	Cr	Ti	Zr	Ta	W	
7	41.45	12.21	20.62	5.66	18.86	1.21	$(Ti, Ta)_5Si_3$
8	44.02	9.55	13.19	21.06	10.63	1.56	ZrSi
9	69.01	0.62	0.83	0.41	26.29	2.85	$TaSi_2$
10	64.90	2.63	2.97	3.30	23.99	2.21	$TaSi_2$
11	65.50	5.05	8.53	5.02	14.58	1.40	$TaSi_2$
12	43.56	26.81	7.79	13.60	6.84	1.40	Cr_5Si_3

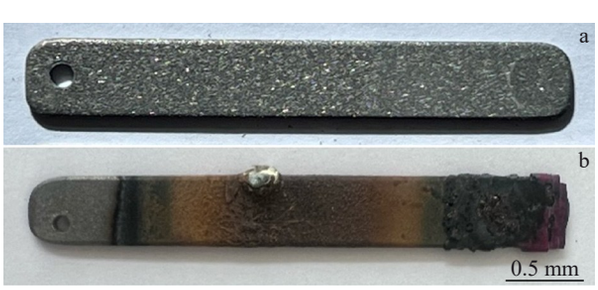

Fig.10 Macroscopic morphologies of Si-Cr-Ti-Zr coatings before (a) and after (b) oxidation at 1600 ℃ for 5 h

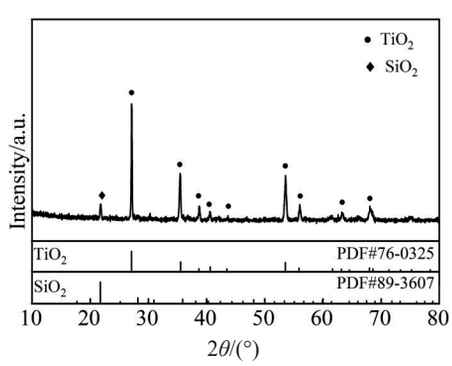

Fig.11 XRD patterns of Si-Cr-Ti-Zr coating after oxidation at 1600 ℃ for 5 h and related composition phase

the miscibility of the silicide ceramics generated by the reactions. To reveal the reaction formation mechanism of the coating, the standard Gibbs free energy ($\Delta_rG_m^\ominus$) of possible reactions was calculated using HSC Chemistry 6 software. The $\Delta_rG_m^\ominus$ curves of possible reactions over the temperature range of 500 – 2000 ℃ are plotted in Fig. 16. Based on the $\Delta_rG_m^\ominus$ value of each reaction, the sequence of reactions during coating formation can be determined, thus clarifying the formation mechanism of the coating. As shown in Fig. 16, the $\Delta_rG_m^\ominus$ values of all potential reactions are negative, indicating

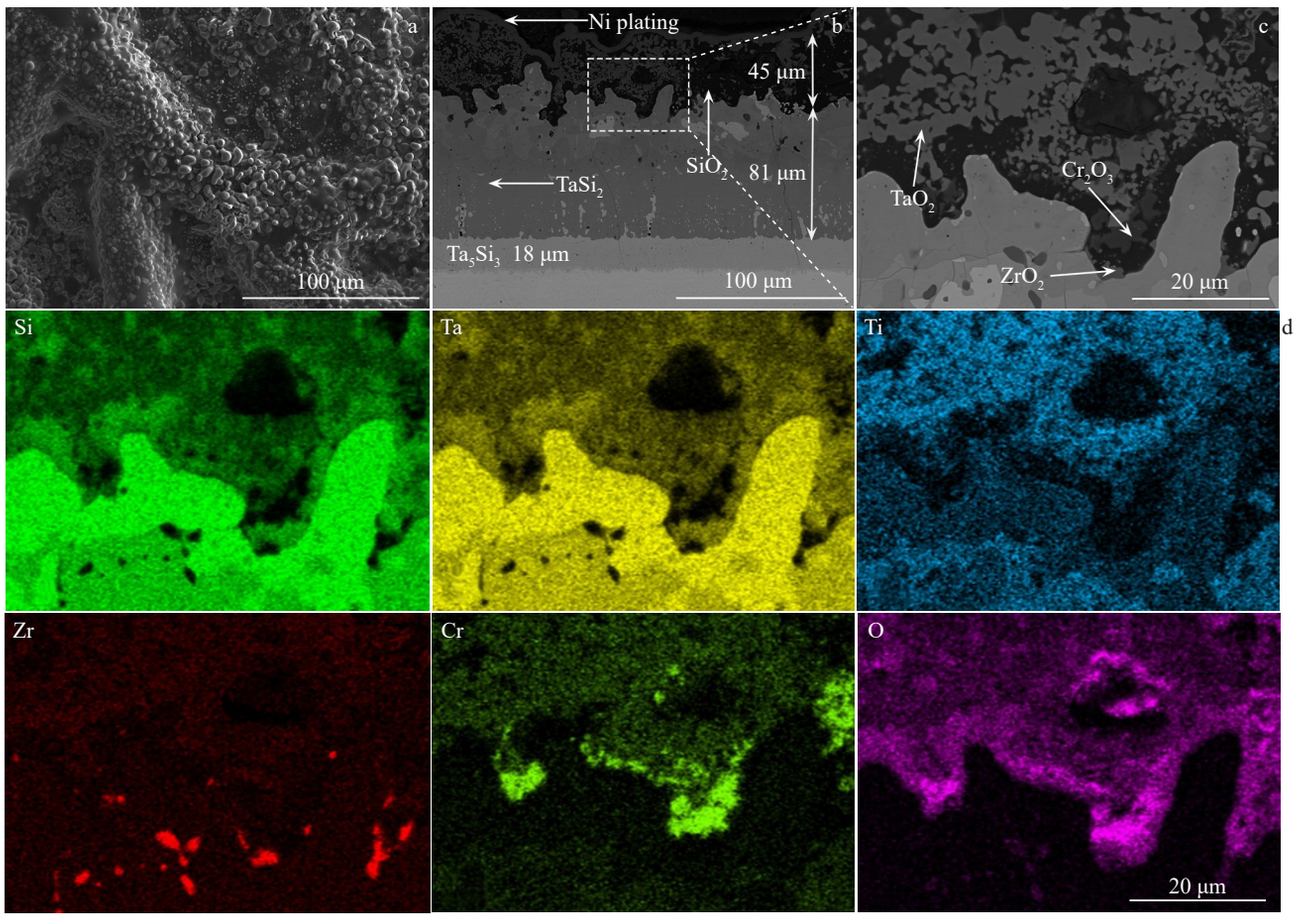

Fig.12 Surface (a) and cross-section (b – c) morphologies of Si-Cr-Ti-Zr coating after oxidation at 1600 ℃ for 5 h; EDS element mappings corresponding to Fig.12c (d)

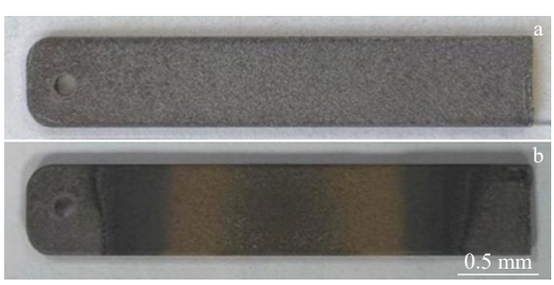

Fig.13 Macroscopic morphologies of Si-Cr-Ti-Zr coatings on Ta12W alloy with MAO pretreatment at 400 V before (a) and after (b) oxidation at 1600 ℃ for 5 h

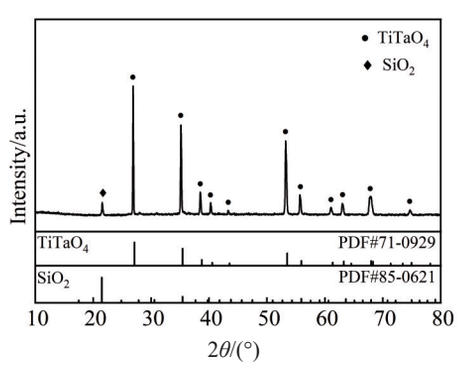

Fig.14 XRD patterns of Si-Cr-Ti-Zr coating on Ta12W alloy with MAO pretreatment at 400 V after oxidation at 1600 ℃ for 5 h and related composition phases

that all these reactions can occur spontaneously at the sintering temperature. The main chemical reactions involved in the coating sintering process are listed in Eq.(1–10):

$$5/3Cr + Si = 1/3Cr_5Si_3 \quad (1)$$

$$1/2Ti + Si = 1/2TiSi_2 \quad (2)$$

$$5/3Ti + Si = 1/3Ti_5Si_3 \quad (3)$$

$$Zr + Si = ZrSi \quad (4)$$

$$1/2Zr + Si = 1/2ZrSi_2 \quad (5)$$

$$1/2Ta + Si = 1/2TaSi_2 \quad (6)$$

$$5/3Ta + Si = 1/3Ta_5Si_3 \quad (7)$$

$$1/7Ta_5Si_3 + Si = 5/7TaSi_2 \quad (8)$$

$$3/7TaSi_2 + Ta = 2/7Ta_5Si_3 \quad (9)$$

$$10/37Ta_2O_5 + Si = 4/37Ta_5Si_3 + 25/37SiO_2 \quad (10)$$

Based on the aforementioned thermodynamic calculation results, combined with the coating cross-section morphologies (Fig. 4) and corresponding EDS area scan results, the in-situ reaction formation mechanism of the as-prepared coating is as follows. Due to its smaller atomic radius (0.117 nm), Si has a

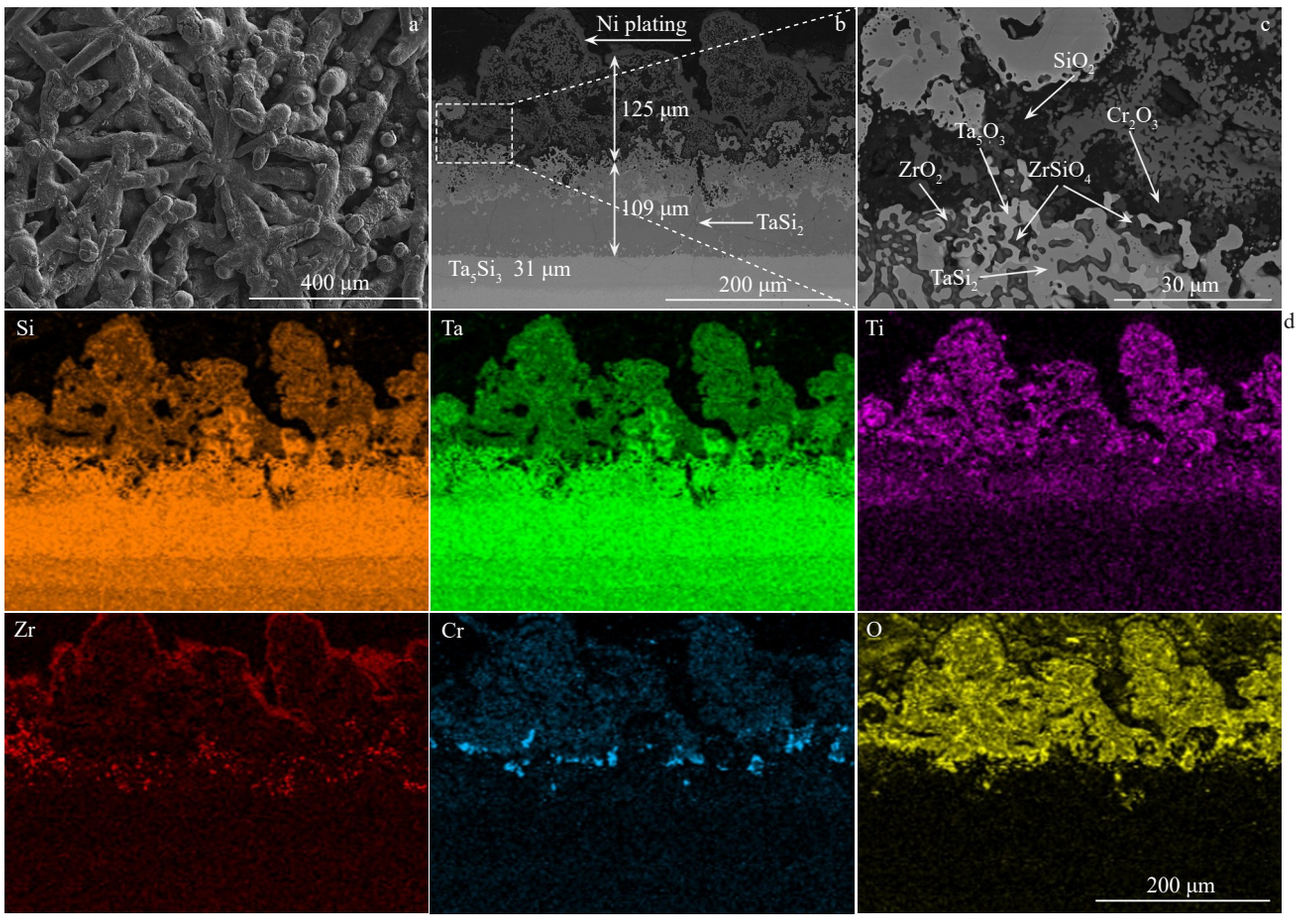

Fig.15 Surface (a) and cross-section (b–c) morphologies of Si-Cr-Ti-Zr coating on Ta12W alloy with MAO pretreatment (400 V) after oxidation at 1600 ℃ for 5 h; EDS element mappings corresponding to Fig.15b (d)

faster diffusion rate than other metal elements in the slurry. Consequently, during the initial stage of coating reaction sintering, the growth of the interfacial reaction layer is controlled by Si diffusion. As clearly shown in Fig. 16, the $\Delta_r G_m^{\ominus}$ for the formation of the Ta_5Si_3 phase is much lower than that for the formation of $TaSi_2$ phase. Therefore, according to Eq. (7), Ta, which continuously diffuses outward from the matrix, reacts with Si, which continuously diffuses inward, initially forming Ta_5Si_3. Simultaneously, active Si atoms continue to diffuse within the coating, thereby increasing the Si atomic concentration in the coating. According to Eq. (8), Ta_5Si_3 continues to react with Si to form $TaSi_2$, which explains the presence of $TaSi_2$ layer (thickness of approximately 50 μm) in the coating. However, as the coating approaches the matrix, the local Ta content increases. Therefore, $TaSi_2$ reacts with matrix-derived Ta to form Ta_5Si_3, according to Eq. (9). Consequently, the main phase of the coating/interfacial reaction layer is Ta_5Si_3.

EDS area scan results in Fig.4b indicate that Ti is uniformly distributed in the main part (outer layer) of the coating. Combined with the thermodynamic data in Fig. 16, this uniform distribution may be attributed to the strong affinity between Ti and Si. Meanwhile, Cr atoms have a smaller atomic radius (0.118 nm) than Zr atoms (0.160 nm), resulting in a higher internal diffusion rate for Cr. During the subsequent sintering process, Cr and Zr diffuse through grain boundaries, leading to the observation of Cr solid solution in the Zr-enriched regions in the main cross-sectional part of the coating. Additionally, due to the low solubility of Cr and Zr in $TaSi_2$, the $TaSi_2$ layer hinders the inward diffusion of Cr and Zr.

After introducing the Ta_2O_5 oxide ceramic diffusion layer, inwardly diffusing Si will react preferentially with Ta_2O_5 to form Ta_5Si_3 and SiO_2, as depicted in Eq. (10). However, the Ta_2O_5 layer has a limited thickness; as Si diffusion continues,

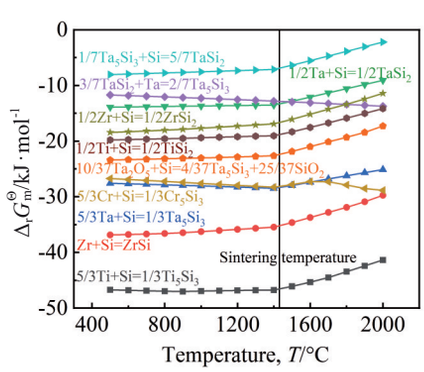

Fig.16 Standard $\Delta_r G_m^{\ominus}$-T curves of possible reactions during coating preparation process

the Ta_2O_5 layer is depleted. Beyond this point, Si will continue to react with Ta in the matrix, following the same mechanism as observed in coatings without the Ta_2O_5 oxide ceramic layer. Therefore, a continuous Ta_2O_5 oxide ceramic layer is not observed in the Si-Cr-Ti-Zr coating after sintering following MAO pretreatment. Since Ta exists in the coating as the Ta-containing compounds Ta_5Si_3/$TaSi_2$, it is rather difficult to measure the specific content of pure Ta in this layer. To determine whether the diffusion of substrate elements is inhibited, the extent of diffusion can be indirectly reflected by the amount of compound formed among Ta and other substrate-related elements. Experimental results show that during the coating preparation process, regardless of the deviation in the thickness of the slurry pre-layer during spraying, comparisons of the thicknesses of the coating/substrate interfacial reaction layers in Fig.4b and Fig.9b reveal distinct differences. In the coating without Ta_2O_5 layer, the proportions of Ta_5Si_3 and $TaSi_2$ are higher of 4.4% and 50%, respectively, and the upward diffusion range of Ta_5Si_3 is larger, accounting for 30%. While in the coating with Ta_2O_5 layer, the proportions of Ta_5Si_3 and $TaSi_2$ are 3.3% and 28%, respectively, which are obviously less, and the diffusion range of Ta_5Si_3 is only 11%. The formation of the Ta_5Si_3 and $TaSi_2$ layers is mainly driven by the diffusion of Si towards the substrate, i. e., the presence of the Ta_2O_5 layer slows down the diffusion of Si towards the substrate side.

4.2 Effect of Ta_2O_5 oxide ceramic layer on oxidation resistance of Si-Cr-Ti-Zr coating

During the isothermal oxidation process of the coating at 1600 °C , the possible chemical reactions involved are as follows.

$$4/27Cr_5Si_3 + O_2(g) = 10/27Cr_2O_3 + 4/9SiO_2 \quad (11)$$

$$1/8Ti_5Si_3 + O_2(g) = 5/8TiO_2 + 3/8SiO_2 \quad (12)$$

$$1/2ZrSi + O_2(g) = 1/2ZrO_2 + 1/2SiO_2 \quad (13)$$

$$1/9Zr_5Si_4 + O_2(g) = 5/9ZrO_2 + 4/9SiO_2 \quad (14)$$

$$5/7TaSi_2 + O_2(g) = 1/7Ta_5Si_3 + SiO_2 \quad (15)$$

$$4/13TaSi_2 + O_2(g) = 2/13Ta_2O_5 + 8/13SiO_2 \quad (16)$$

$$Ta + 5TiO_2 + 2Ta_2O_5 = 5TiTaO_4 \quad (17)$$

$$ZrO_2 + SiO_2 = ZrSiO_4 \quad (18)$$

$$ZrSiO_4 = ZrO_2 + SiO_2 \quad (19)$$

Based on the standard $\Delta_rG_m^{\ominus}$-T curves of possible reactions during the oxidation process (Fig. 17), the oxygen affinity potential of Ti is significantly higher than that of Si, Cr, Ta, and other elements in the system. Additionally, there is a large amount of Ti_5Si_3 phase on the coating surface. This suggests that Ti_5Si_3 on the coating surface will preferentially react with oxygen to form TiO_2 and SiO_2, according to Eq. (12). According to SiO_2-TiO_2 phase diagram (Fig. 18), SiO_2 and TiO_2 do not undergo chemical reactions and are immiscible in the solid state, thus forming a composite oxide film. This film mainly consists of amorphous SiO_2, which exhibits excellent oxygen-blocking performance. Meanwhile, the SiO_2 layer is reinforced by high-melting-point crystalline TiO_2 oxide, resulting in a typical “sand-stone” concrete-like micro-

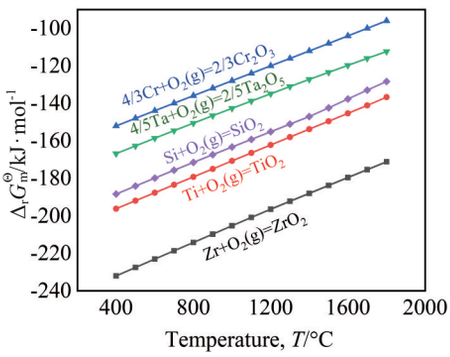

Fig.17 $\Delta_rG_m^{\ominus}$-T curves of possible reactions during coating oxidation process

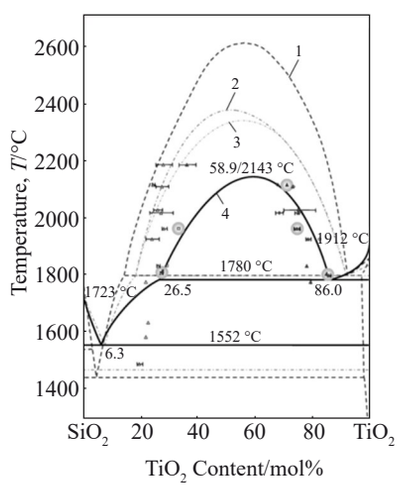

Fig.18 Phase diagram of the SiO_2-TiO_2 system[29]

structural characteristic. As O_2 continues to diffuse inward, it reacts with Cr and Zr in the outer part of the coating to generate Cr_2O_3 and ZrO_2, according to Eq. (11) and Eq. (13), respectively. Simultaneously, oxygen diffuses further into the coating interior, and it reacts with $TaSi_2$ to consume this phase and produce SiO_2 and Ta_5Si_3, according to Eq. (15). Therefore, the Ta_5Si_3 layer thickens after the coating is oxidized.

Unlike the coating without the Ta_2O_5 oxide ceramic layer, no crystalline TiO_2 was found on the surface of the coating with the Ta_2O_5 layer. This absence may be due to the reaction between Ta_2O_5 and TiO_2, as shown in Eq. (17). Additionally, the presence of $ZrSiO_4$ was observed, which may be attributed to the reaction between ZrO_2 and SiO_2, as shown in Eq. (18). $ZrSiO_4$ not only provides particle reinforcement in the molten SiO_2 oxide film, but also adjusts the coefficient of thermal expansion (CTE) of the oxide scale (CTE_{ZrO_2}=10.6×10^{-6} K^{-1}, CTE_{ZrSiO_4}=4.9×10^{-6} K^{-1}, and CTE_{SiO_2}=0.5×10^{-6} K^{-1}), thereby reducing the thermal stress during oxidation. However, the generated $ZrSiO_4$ is thermally unstable. Once the temperature reaches 1500 °C, a portion of $ZrSiO_4$ will decompose into ZrO_2 and SiO_2[30].

For the Si-Cr-Ti-Zr coating without the Ta_2O_5 oxide ceramic layer, during the oxidation process, the elements in the coating

and Ta in the substrate mutually diffuse, leading to rapid diffusion and consumption of Si. This results in a transformation of the main phase of the coating from $TaSi_2$ to Ta_5Si_3, which has lower Si content and does not exhibit excellent high-temperature oxidation resistance. Therefore, due to Si depletion, the generated SiO_2 is insufficient to form a continuous protective film covering the entire specimen surface, allowing oxygen to penetrate the coating interior along gaps. Compared to the coating without the Ta_2O_5 oxide ceramic layer, the presence of the Ta_2O_5 oxide ceramic layer inhibits the high-temperature diffusion and consumption of Si atoms from the coating toward the substrate, thereby enhancing the high-temperature oxidation resistance of the Si-Cr-Ti-Zr coating.

5 Conclusions

1) A Ta_2O_5 oxide layer is prepared on the Ta12W substrate via MAO method. Compared with the layer prepared at 350 V, the Ta_2O_5 layer prepared at 400 V is more continuous and has smaller pore sizes.

2) A Si-Cr-Ti-Zr coating is prepared on the MAO-pretreated Ta12W surface using a slurry spraying-vacuum reaction sintering method. The coating features a three-layer structure: an upper layer with Ti_5Si_3, Ta_5Si_3, and ZrSi as the main phases; a middle layer, primarily composed of the $TaSi_2$ phase; a coating/substrate interfacial reaction layer with Ta_5Si_3 as the main phase.

3) Both the Si-Cr-Ti-Zr coatings with and without the Ta_2O_5 ceramic layer on the Ta12W surface do not fail after isothermal oxidation at 1600 ℃ for 5 h. Notably, the addition of the Ta_2O_5 oxide ceramic layer can reduce the high-temperature oxidation rate of the coating.

References

1 Wang X, Xin K X, Li Q Y *et al. International Journal of Refractory Metals and Hard Materials*[J], 2023, 113: 106189

2 La M, Qin L, Wang L L *et al. Applied Surface Science*[J], 2024, 661: 160085

3 Liu S, Shen H, Xu J *et al. Journal Materials Science & Technology*[J], 2021, 81: 117

4 Zhang G, Sun J, Fu Q *et al. Surface and Coatings Technology*[J], 2020, 400: 126210

5 Liu L, Zhang H Q, Lei H *et al. Ceramics International*[J], 2020, 46: 5993

6 Zhu L, Zhang S P, Ye F *et al. Composites Part B: Engineering*[J], 2024, 274: 111281

7 Bu X J, He P F, Zhang P *et al. Corrosion Science*[J], 2024, 237: 112316

8 Xu J W, Xiao L R, Zhang Y F *et al. Corrosion Science*[J], 2023, 224: 111563

9 Xu Y, Zheng W, Dai M *et al. Journal of the European Ceramic Society*[J], 2023, 43(14): 5802

10 Zhang Y, Yu L, Fu T *et al. Surface and Coatings Technology*[J], 2022, 431: 128037

11 Wang Z, Wang Y, Wang S *et al. Corrosion Science*[J], 2022, 206: 110460

12 Zhang Y F, Liu S N, Zhou X *et al. Corrosion Science*[J], 2022, 195: 109977

13 Hou Q Y, Shao W, Li M F *et al. Surface Coatings Technology*[J], 2020, 401: 126243

14 Li S, Xiao L R, Liu S N *et al. Journal of the European Ceramic Society*[J], 2022, 42: 4866

15 Li H, Yu Y, Fang B *et al*. *Journal of the European Ceramic Society*[J], 2022, 42(11): 4651

16 Liu Q, Hu X, Zhu W *et al*. *Journal of the American Ceramic Society*[J], 2021, 104(12): 6533

17 Cheng C Y, Lv T T, Song B H *et al. Surface and Interfaces*[J], 2024, 53: 105050

18 Ye Z, Zou Y, Wang S *et al*. *Corrosion Science*[J], 2024, 230: 111908

19 Su R, Zhang H, Ouyang G *et al. Acta Materialia*[J], 2023, 246: 118719

20 Fu T, Cui K K, Zhang Y Y *et al. Journal of Alloys and Compounds*[J], 2021, 884: 161057

21 Cheng C, Xie W, Li H *et al. Journal of the American Ceramic Society*[J], 2021, 104(7): 3130

22 Wang S Q, Ye Z Y, Ge Y L *et al. Journal of Materials Research and Technology*[J], 2021, 210: 159

23 Wang C L, Shao W, Wang W *et al. Corrosion Science*[J], 2020, 163: 108249

24 Zhai J K, Ma X, Bai X D *et al. Acta Aeronautica et Astronautica Sinica*[J], 1994, 15(4): 499

25 Yue G, Guo X P, Qiao Y Q *et al. Applied Surface Science* [J], 2020, 504: 144477

26 Cai Z Y, Zhao X J, Zhang D X *et al. Corrosion Science*[J], 2018, 143: 116

27 Dai W B, Zhang X L, Li C Y *et al. Surface Engineering*[J], 2021, 360: 4

28 Pecherskaya E A, Golubkov P E, Artamonov D V. *IEEE Transactions on Plasma Science*[J], 2021, 490: 2613

29 Li D L, Li C W, Chen H. *Materials Chemistry and Physics*[J], 2022, 290: 126598

30 Wang X, Zhang W, Wang T Y *et al. Corrosion Science*[J], 2025, 251: 112914

基材微弧氧化预处理对Ta12W表面Si-Cr-Ti-Zr涂层组织结构及抗高温氧化性能的影响

杨　凡[1,2]，常剑秀[1]，汪　欣[2]，李宏战[2]，严　鹏[2]

(1. 西安石油大学 材料科学与工程学院，陕西 西安 710065)

(2. 西北有色金属研究院，陕西 西安 710016)

摘　要：为了降低真空熔烧反应过程中硅化物料浆与Ta12W合金基体互扩散反应对硅化物涂层抗氧化性能的影响，采用微弧氧化预处理工艺在Ta12W合金表面构建Ta_2O_5陶瓷层，随后采用料浆喷涂-真空反应烧制方法在预处理后的基体表面制备Si-Cr-Ti-Zr涂层，对比研究有/无微弧氧化陶瓷层的制备态涂层的显微组织结构、物相组成以及1600 ℃的恒温抗氧化性能。结果表明，400 V电压下制备的Ta_2O_5氧化物陶瓷层相对于350 V更为连续且孔隙更小；微弧氧化后Ta12W合金表面Si-Cr-Ti-Zr涂层由以Ti_5Si_3、Ta_5Si_3和ZrSi为主相的上层，以$TaSi_2$为主相的中层，以及以Ta_5Si_3为主相的涂层/基体界面反应层组成；有/无Ta_2O_5陶瓷层的Si-Cr-Ti-Zr涂层在1600 ℃下恒温氧化5 h后未发生失效，但Ta_2O_5氧化物陶瓷层的添加可以延缓涂层的高温氧化速率。

关键词：钽钨合金；硅化物涂层；微弧氧化；反应形成机制；高温氧化

作者简介：杨　凡，女，1999年生，硕士，西安石油大学材料科学与工程学院，陕西 西安 710065，E-mail：15389210253@163.com